Photon-momentum transfer in one- and two-photon ionization of atoms

Mu-Xue Wang,[1] Xiang-Ru Xiao,[1] Hao Liang,[1] Si-Ge Cheng,[1] and Liang-You Peng[1,2,*]

[1]*State Key Laboratory for Mesoscopic Physics and Collaborative Innovation Center of Quantum Matter, School of Physics, Peking University, Beijing 100871, China*

[2]*Collaborative Innovation Center of Extreme Optics, Shanxi University, Taiyuan, Shanxi 030006, China*

(Received 15 July 2017; published 17 October 2017)

The transfer of the linear photon momentum to the electron in the few-photon ionization of an atom is accurately computed through a numerical solution to the three-dimensional time-dependent Schrödinger equation (TDSE) beyond the dipole approximation. The characteristics of the transfer is studied in detail by comparing the TDSE results with those calculated by the perturbation theory (PT) using the exact scattering states. Our fully quantum-mechanical calculations show a discernible photoelectron momentum shift along the laser's propagation direction, which is caused by the nondipole effects. The momentum transfer rule for the single-photon ionization is shown to agree with results obtained from the perturbation theory. We identify some extraordinary "dips" in the photon-momentum transfer in the case of two-photon ionization, which depend on the laser ellipticity and are caused by the suppression of the nondipole transitions. In addition, the Coulomb screening effect on the photon-momentum transfer has also been investigated and we find that the Coulomb tail is negligible in the single-photon ionization case. However, the potential in the short range near the Coulomb center may influence the initial state, which will change the amount of the momentum that can be transferred.

DOI: 10.1103/PhysRevA.96.043414

I. INTRODUCTION

In many theoretical descriptions of the interaction between strong fields and atoms or molecules, the electric dipole approximation has been widely used. Under this approximation, laser fields are treated as homogeneous time-dependent electric fields and the dependence of the vector potential on spatial coordinates as well as the homogeneous magnetic field components are assumed to be negligible. In fact, the dipole approximation applies only in a limited frequency and intensity range. When approaching the well-known short- or long-wavelength dipole limit [1–3], the dipole approximation will break down and nondipole corrections are bound to be considered.

Nondipole effects are usually associated with very high laser intensities or very large laser frequencies, which play a significant role in the study of strong-field atomic stabilization occurring in the single-electron photoionization [4–9] or in two-electron systems [10,11]. Nondipole effects in photoelectron angular distributions have also been investigated. Besides the forward or backward asymmetry of the angular distributions in the soft-x-ray region [12–19], unique nondipole lobe structures were theoretically predicted for both the hydrogen atom [20–22] and H_2^+ [23]. Some research groups also paid attention to the analysis of asymmetries of the triply differential cross section induced by the nondipole corrections in the double ionization of atoms [24–26] as well as the contributions of the nondipole corrections to the photoelectron spin polarization [27–29] based on the single-active-electron approximation. Among the investigations about the nondipole effects, the photon-momentum transfer in ionization ranging from the perturbation regime to the tunneling regime has attracted increasing attention recently [30–44].

Due to the extreme smallness of linear momentum of a single visible photon, it is usually neglected in the strong field physics. With the development of highly sensitive measuring instruments, Smeenk *et al.* [30] and Ludwig *et al.* [36] have successively reported experimental observation of photoelectron momentum shift along the direction of laser propagation in the tunneling ionization processes. Theoretical works have confirmed this asymmetrical [36,42] electron momentum distribution and a nonzero momentum shift along the laser's propagation direction by quantum-mechanical calculations [31,38], using semiclassical models with the Lorentz force included [34,36,42], through solving the time-dependent Dirac equation [39], or by strong field approximation (SFA) models beyond the dipole approximation [37,43]. The pioneering work from Chelkowski *et al.* [37] has revealed different photon-momentum partitioning rules for one-photon ionization and multiphoton processes, which has been supported by a recent study [43]. In the linearly polarized long-wavelength limit, the Coulomb interaction and the rescattering may result in a momentum shift opposite to the direction of laser propagation [36,42,43], particularly for the low-energy electrons. Besides, the underbarrier motion caused by the laser-magnetic-field-induced Lorentz force has been reported to be relevant with the electron momentum shift in the laser propagation direction [32,35,40].

The photon-momentum transfer in the ionization process is assumed to be one kind of the nondipole effects and plays a significant part in characterizing the radiation pressure. However, most previous theoretical and experimental work paid much attention to the tunneling process in the high-intensity and long-wavelength limit. Here we solve the three-dimensional (3D) time-dependent Schrödinger equation (TDSE) beyond the dipole approximation for a single-electron system interacting with a very long UV (or XUV) pulse in the nonrelativistic regime. To the best of our knowledge, we provide the most detailed *ab initio* simulations of photon-momentum transfer in the few-photon ionization region. Our fully quantum-mechanical calculations show a good linear relationship between the average kinetic energy of

*liangyou.peng@pku.edu.cn

photoelectrons $\langle E_k \rangle$ and the expectation value of the electron momentum along laser propagation direction $\langle p_z \rangle$ in the case of the single-photon ionization. Most notably we discover some interesting new features of this relationship for the two-photon ionization process, e.g., some characteristic "dips" appear at specific laser frequencies, which have never been observed before. We attribute this to the suppression of some nondipole transitions. Finally, we also discuss the Coulomb screening effect on the transfer of photon momentum for the aforementioned cases by the perturbation theory. Results of hydrogen and helium atoms in different short-range potentials are compared and discussed.

The rest of the paper is organized as follows. In Sec. II we start by introducing our numerical methods of solving the TDSE. Then in Sec. III we will compare our TDSE calculations in the single-photon case with the results obtained from the perturbation theory, followed by the presentation and discussion for the two-photon absorption case in Sec. IV. We will address in Sec. V the influence of the Coulomb screening effect in the momentum transfer. A short conclusion is drawn in Sec. VI. Atomic units are employed throughout the paper unless otherwise stated.

II. NUMERICAL METHODS

In the nonrelativistic situation, the dynamics of a hydrogen atom interacting with a classical electromagnetic field can be described by the time-dependent Schrödinger equation

$$i\frac{\partial}{\partial t}\Psi(\mathbf{r},t) = H\Psi(\mathbf{r},t), \tag{1}$$

where the full Hamiltonian in the velocity gauge is given by

$$H = \tfrac{1}{2}[\mathbf{p} + \mathbf{A}(\mathbf{r},t)]^2 + V(\mathbf{r}). \tag{2}$$

With the inclusion of only the lowest order of the nondipole corrections [40,45–47], the time- and space-dependent vector potential $\mathbf{A}(\mathbf{r},t)$ for a circularly polarized light field propagating in the positive z axis can be written as

$$\mathbf{A}(\mathbf{r},t) = A_x(z,t)\mathbf{e}_x + A_y(z,t)\mathbf{e}_y, \tag{3}$$

$$A_x(z,t) \simeq A_x(t) + \frac{z}{c}E_x(t), \tag{4}$$

$$A_y(z,t) \simeq A_y(t) + \frac{z}{c}E_y(t), \tag{5}$$

in which $A_x(t)$ and $A_y(t)$ are components of the vector potential in the dipole approximation, $E_x(t)$ and $E_y(t)$ are the corresponding electric fields, and c is the vacuum light speed.

Inserting the vector potential into Eq. (2), we can get the leading-order corrected nondipole Hamiltonian

$$\begin{aligned} H_{\text{nondipole}} = &-\tfrac{1}{2}\nabla^2 + V(r) - iA_x(t)\partial_x - iA_y(t)\partial_y \\ &- i\frac{z}{c}E_x(t)\partial_x - i\frac{z}{c}E_y(t)\partial_y \\ &+ \frac{z}{c}A_x(t)E_x(t) + \frac{z}{c}A_y(t)E_y(t). \end{aligned} \tag{6}$$

Here we focus on the hydrogenlike system and the ionic potential is spherically symmetric, $V(\mathbf{r}) = V(r)$. Note that the purely time-dependent term $A^2(t)/2$ has been dropped as it can be taken away by a phase transformation and has no effect on any of the potentials and observables.

To solve the TDSE, the wave function $\Psi(\mathbf{r},t)$ is expanded in the spherical harmonics $Y_{lm}(\theta,\phi)$ for the angular coordinates, which leads to a set of coupled equations for the radial wave functions,

$$\Psi(\mathbf{r},t) = \sum_{l=0}^{\infty}\sum_{m=-l}^{l}\frac{\Phi_{lm}(r,t)}{r}Y_{lm}(\theta,\phi). \tag{7}$$

The resultant Schrödinger equation for the radial coefficients Φ_{lm} can be solved using various discretization methods [48,49]. In the present work, we use the finite difference for the radial coordinate and the split-operator technique for the short-time propagator [50]. The initial state is obtained by an imaginary time propagation in the absence of the external field until the ground-state energy is fully converged.

After the end of the external fields, we get the final wave function Ψ_f and project it onto the scattering states given by Eq. (4.27) in Ref. [51]:

$$\begin{aligned} \Psi_{\mathbf{p}}^{-}(\mathbf{r}) &= \frac{1}{\sqrt{p}}\sum_{l,m} i^l e^{-i(\sigma_l+\delta_l)}Y_{lm}^*(\theta,\phi)R_{El}(r)Y_{lm}(\theta',\phi') \\ &= \frac{1}{\sqrt{2\pi}\,p}\sum_{l,m} i^l e^{-i(\sigma_l+\delta_l)}Y_{lm}^*(\theta,\phi)R_{pl}(r)Y_{lm}(\theta',\phi'), \end{aligned}$$

in which the factors $\frac{1}{\sqrt{p}}i^l e^{-i\delta_l}$ ensure the wave boundary condition as well as the normalization condition to be satisfied, and $\sigma_l = \arg\Gamma(l+1-i/p)$ is the Coulomb phase shift. Then the probability of the electron with a final momentum $\mathbf{p} = (p,\theta',\phi')$ is given by

$$\begin{aligned} P(p,\theta',\phi') = |\langle\Psi_{\mathbf{p}}^{-}|\Psi_f\rangle|^2 &= \left|\frac{1}{\sqrt{2\pi}\,p}\sum_{l,m}\int_0^{\infty} dr(-i)^l e^{i(\sigma_l+\delta_l)}\right. \\ &\quad \left.\times\, r R_{pl}(r)\Phi_{lm}(r)Y_{lm}(\theta',\phi')\right|^2 \\ &= \left|\sum_{l,m} C_{lm}Y_{lm}(\theta',\phi')\right|^2. \end{aligned} \tag{8}$$

In this way the final wave function in the momentum space is expanded in partial waves. We define the weight of each partial wave as

$$W_{lm} = |C_{lm}|^2. \tag{9}$$

For the purpose of the present work to investigate the photon-momentum transfer along the z axis, one needs to extract the photoelectron momentum $f(p_z)$ along the laser propagation direction. For convenience, the above 3D photoelectron momentum distribution has been changed from the spherical coordinates (p,θ',ϕ') to the cylindrical coordinates (p_ρ,p_z,ϕ') with a very high accuracy through the method of Gouraud shading [52]. The electron momentum distribution along the laser propagation direction is then calculated by

$$f(p_z) = \iint P(p_\rho,p_z,\phi')p_\rho dp_\rho d\phi', \tag{10}$$

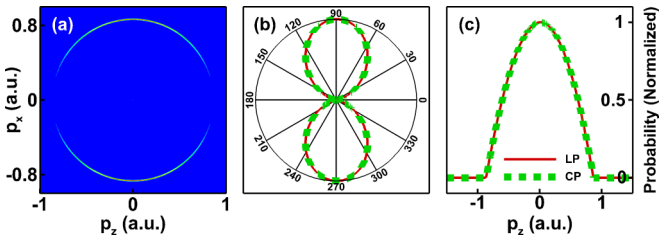

FIG. 1. (a) The 2D photoelectron momentum distribution in the xz plane of a hydrogen atom by a linearly polarized laser along the x axis. (b) The normalized angular distributions in the xz plane for both the linear (red solid line) and the circular (dashed green line) polarization. (c) The normalized photoelectron momentum distribution $f(p_z)$ along the laser propagation direction. See the text for the laser parameters.

from which one can calculate the electron average momentum $\langle p_z \rangle$ as follows:

$$\langle p_z \rangle = \frac{\int p_z f(p_z) dp_z}{\int f(p_z) dp_z}. \tag{11}$$

Apparently, $\langle p_z \rangle$ is the photon linear momentum that has been transferred to the photoelectron.

For our cases, convergences are easy to be ensured with respect to the basis size $l_{\max} = 8$ because of the relatively weak fields ($\sim 10^{13}$ W/cm^2). But we need a large radial box $r_{\max} = 12\,000$ with $\Delta r = 0.1$ for our long XUV pulses ($\sim$10fs). A parallel computing method has been used to increase the efficiency of our calculations.

III. ONE-PHOTON IONIZATION CASE

First, we will discuss the radiation pressure effects in the one-photon ionization process. We use the following Gaussian laser pulses propagating in the positive z direction: $\omega = 0.875$ a.u., the pulse duration is around 10 fs, and the intensity is 5×10^{12} W/cm^2 for the linear polarization case and 1×10^{13} W/cm^2 for the circular polarization case.

In Fig. 1(a) we present the two-dimensional (2D) photoelectron momentum distribution (which is the cut with $p_y = 0$ for our actual 3D momentum distribution) in the linear polarization laser case. We show the angular distributions for both the linear polarization (LP) and the circular polarization (CP) case in Fig. 1(b). The electron momentum distribution along the laser propagation direction calculated from Eq. (10) is shown in Fig. 1(c) for both cases. From these figures, one can see that the differential distributions are independent on the laser polarization.

Figure 2 shows the electron average momentum $\langle p_z \rangle$ as a function of the laser frequency for both the linear and circular polarization. There seems to be no discernible difference between results from the LP pulses and the CP pulses in Figs. 1 and 2 for the single-photon case. Due to the significantly long pulse that we have used, we can see that the average electron kinetic energy $\langle E_k \rangle$ is exactly equal to $\omega - I_p$ where I_p is the ionization potential. The red open circles, the green solid deltas, and the black dashed line confirm

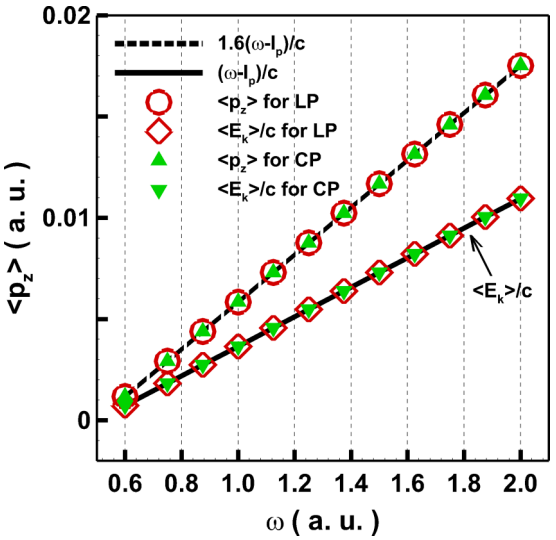

FIG. 2. The expectation of photoelectron momentum $\langle p_z \rangle$ along the laser propagation direction as a function of the laser frequency ω in the single-photon ionization regime. Red open circles (green solid regular triangles): $\langle p_z \rangle$ for the LP (CP) light. Red open diamonds (green solid inverted triangles): the electron average kinetic energy $\langle E_k \rangle$ divided by the vacuum light speed c for the LP (CP) light. Black dashed line: the momentum transfer law given by the analytic first-order perturbation theory in Eq. (12). Black solid line: $(\omega - I_p)$ divided by the vacuum light speed c.

the momentum transfer law proposed in Ref. [37] for both the linear polarization and the circular polarization,

$$\langle p_z \rangle = \frac{8}{5}\frac{\langle E_k \rangle}{c} = \frac{8}{5}\frac{(\omega - I_p)}{c}. \tag{12}$$

IV. TWO-PHOTON IONIZATION CASE

Now we will discuss the photon-momentum transfer in the two-photon ionization. Laser parameters are the same with the single-photon ionization case except for laser frequencies. However, obvious discrepancies appear between the results with linearly polarized fields and those with circularly polarized fields in the two-photon ionization process.

Similar to Fig. 1 for the one-photon case, in Fig. 3 we show the 2D photoelectron momentum distribution for a linearly polarized field, corresponding angular distributions, and distributions along the laser propagation direction for both the LP and the CP cases, at $\omega = 0.4$ a.u. (top panel) and $\omega = 0.425$ a.u. (lower panel). First of all, we observe strikingly different features in the 2D momentum distributions at both photon energies, i.e., a circle in Fig. 3(a) and a four-lobe structure in Fig. 3(d). In fact, one can find significant differences between the results from the LP and CP cases in the angular distributions shown in Figs. 3(b) and 3(e): it seems that the angular distribution for the CP case is insensitive to the photon energy while it strongly depends on the photon energy for the LP case.

The differences at these two frequencies are due to different weights of the partial waves, in which the final wave function in the momentum space is expanded in Eq. (8). These lm partial waves come from different transition channels and

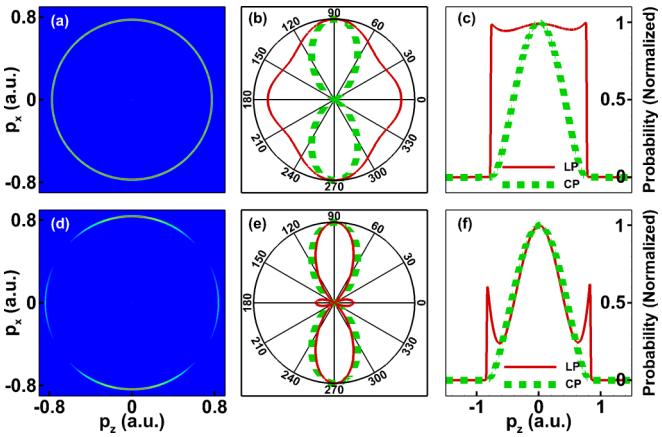

FIG. 3. Same as those of Fig. 1, but for the two-photon ionization case at two different frequencies $\omega = 0.4$ a.u. (first row) and $\omega = 0.425$ a.u. (second row).

we can obtain their weights from Eq. (9), as is shown in Fig. 4. We can temporally forget the nondipole corrections here to simply explain the strikingly different features in Fig. 3. According to the selection rules, the intermediate states are only p states (the $l = 1$, $m = \pm 1$ partial waves) and the final wave function consists of the $l = 0, m = 0$ partial wave and the $l = 2, m = 0, \pm 2$ partial waves under the dipole approximation. The $l = 0, m = 0$ partial wave produces the circle structure, the $l = 2, m = 0$ partial wave produces the four-lobe structure, and the $l = 2, m = \pm 2$ partial waves are related to the two-lobe structure in the momentum space. In the first row of Fig. 4, no significant difference was found

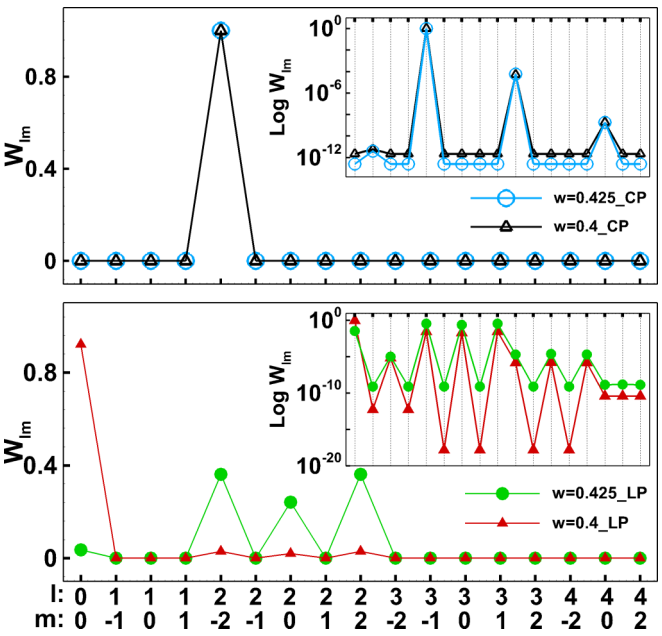

FIG. 4. The weight of each partial wave. Black solid line with open triangles (blue solid line with open circles) in the first row: W_{lm} in the CP field of the frequency $\omega = 0.4$ a.u. ($\omega = 0.425$ a.u.); red solid line with solid triangles (green solid line with solid circles) in the second row: W_{lm} in the LP field of the frequency $\omega = 0.4$ a.u. ($\omega = 0.425$ a.u.). Inset: W_{lm} in the log scale.

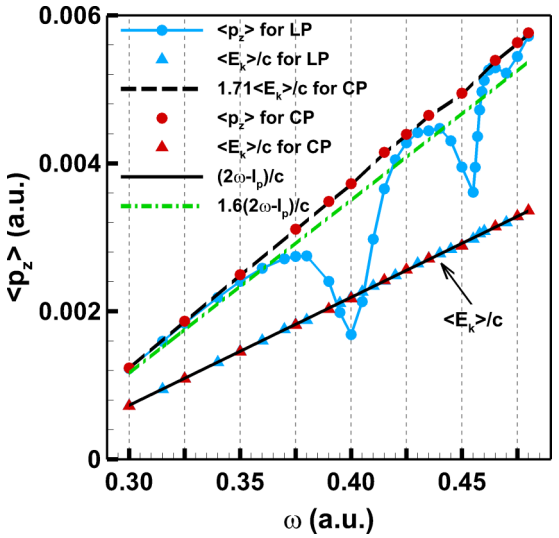

FIG. 5. The expectation of photoelectron momentum $\langle p_z \rangle$ along the laser propagation direction as a function of the laser frequency ω in the two-photon ionization regime. Red solid circles (blue solid line with circles): $\langle p_z \rangle$ for the CP (LP) light. Red (blue) triangles: $\langle E_k \rangle / c$ for the CP (LP) light. Black dashed line: $1.71(2\omega - I_p)/c$. Black solid line: $(2\omega - I_p)/c$.

in the weights of the partial waves at these two frequencies in the case of circularly polarized fields, in which the $l = 2, m = -2$ partial wave apparently dominates and so their angular distributions are both like the number "8" in Figs. 3(b) and 3(e). However, in the case of linearly polarized fields, the $l = 2, m = 0$ partial wave and the $l = 2, m = \pm 2$ partial waves dominate at the frequency $\omega = 0.425$ a.u., while the $l = 0, m = 0$ partial wave dominates at $\omega = 0.4$ a.u., which can explain the four-lobe structure in Fig. 3(d) and the circle structure in Fig. 3(a). These differences are also exhibited in the $f(p_z)$ distributions in Fig. 3(c) and 3(f) so the momentum expectation value $\langle p_z \rangle$ will certainly be affected.

In Fig. 5 we plot $\langle p_z \rangle$ as a function of the laser frequency for the two-photon ionization case. For circularly polarized lasers, there still exists a good linear relationship between $\langle p_z \rangle$ and ω. It is worth noting that the momentum transfer law becomes closer to

$$\langle p_z \rangle = 1.71 \frac{\langle E_k \rangle}{c} = 1.71 \frac{(2\omega - I_p)}{c}, \tag{13}$$

which is slightly different from $\langle p_z \rangle = 1.6 \langle E_k \rangle / c$ for the single-photon ionization case. A similar relationship was also found recently in Ref. [44]. We agree with the point that the slight increase of the slope is related to the second transition starting from the intermediate p and d states and the one-photon radiative pressure effect from these states increases [44,53]. This has also been confirmed in Fig. 6, in which we present $\langle p_z \rangle$ as a function of $\langle E_k \rangle / c$ for different initial states, i.e., $1s, 2s, 2p\,(m = 0), 2p\,(m = -1), 2p\,(m = 1)$, or $3d$ state, all interacting with a circularly polarized laser field.

Another interesting phenomenon in Fig. 5 is that $\langle p_z \rangle$ for the linear polarization case exhibits some dips around some particular frequencies, e.g., $\omega = 0.4$ a.u. and $\omega = 0.455$ a.u., which has never been reported before. These unusual dips

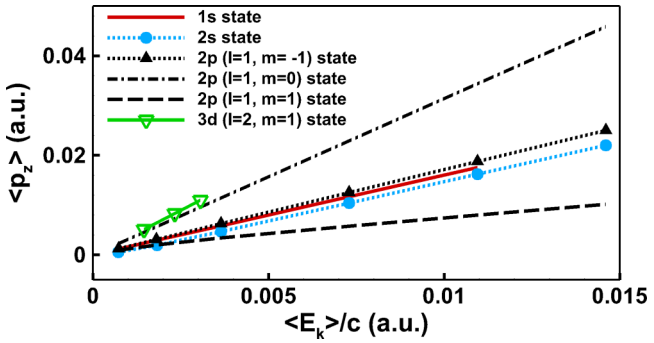

FIG. 6. The expectation of photoelectron momentum $\langle p_z \rangle$ along the laser propagation direction as a function of $\langle E_k \rangle/c$ in the one-photon ionization regime with different initial states: red solid line for the $1s$ (angular quantum number $l = 0$ and magnetic quantum number $m = 0$) state; blue dotted line with solid circles for the $2s$ ($l = 0, m = 0$) state; black dash-dotted line for the $2p$ ($l = 1, m = 0$) state; black dotted line with solid triangles for the $2p$ ($l = 1, m = -1$) state; black dashed line for the $2p$ ($l = 1, m = 1$) state; green solid line with open inverted triangles for the $3d$ ($l = 2, m = 1$) state.

disappear for circularly polarized cases. Besides, we find that the depth of these dips will decrease with the increase of the laser field ellipticity, as is shown in Fig. 7 for $\omega = 0.4$ a.u. Note that $\langle p_z \rangle$ increases with the laser field ellipticity but $\langle E_k \rangle/c$ keeps almost unchanged at the same time. In other words, the dip at $\omega = 0.4$ a.u. in Fig. 5 gradually diminishes when the laser is continuously changed from the linear polarization to the circular polarization. This is different from the case of the single-photon ionization discussed before, in which $\langle p_z \rangle$ is independent of the laser ellipticity.

We attribute these unique features to the different weights of the partial waves related to the nondipole transitions, which appear with the nondipole corrections considered and follow different selection rules from the dipole parts. We call those following the selection rules under the dipole approximation as dipole transitions.

Specifically, the intermediate state after absorbing the first photon will be comprised of the $l = 1, m = \pm 1$ partial waves from the dipole transitions and the $l = 1, m = 0$ partial wave and the $l = 2, m = \pm 1$ partial waves from the nondipole transitions. Then the second transition starting from this

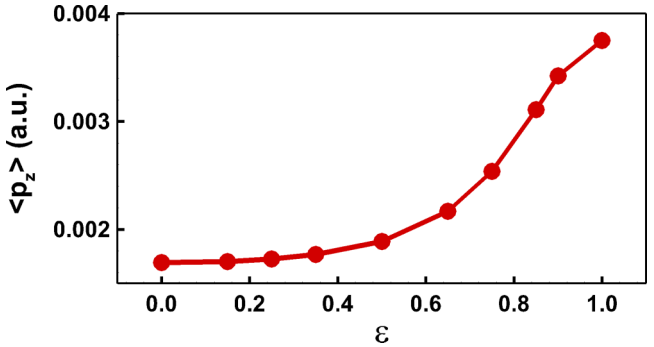

FIG. 7. The expectation of photoelectron momentum $\langle p_z \rangle$ along the laser propagation direction as a function of the laser ellipticity ε at $\omega = 0.4$ a.u.

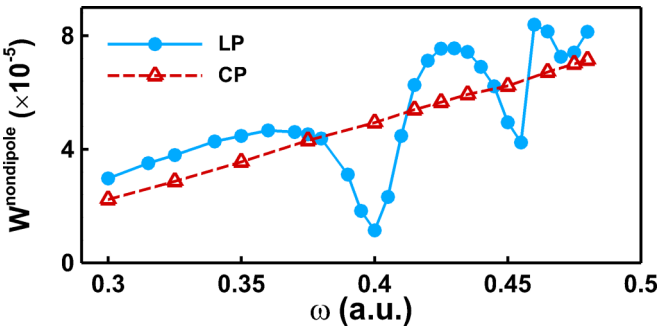

FIG. 8. The total weight of partial waves related to the nondipole transitions at different laser frequencies. Blue solid line with circles (red dashed line with triangles): $W^{\text{nondipole}}$ for the LP (CP) pulse.

intermediate state will result in a final state which can be expanded in partial waves related to the dipole or nondipole transitions. We only focus on the nondipole ones with their weights marked as $W_{lm}^{\text{nondipole}}$, which do not exist under the dipole approximation, such as the $l = 1, m = \pm 1$ and $l = 2, m = \pm 1$ partial waves, etc. We denote the total weight as $W^{\text{nondipole}} = \sum_{l,m} W_{lm}^{\text{nondipole}}$.

It is reasonable to quantify the nondipole effect with $W^{\text{nondipole}}$, which is shown in Fig. 8 at varied laser frequencies both for the linear and circular polarization. We can see a series of minimum points in Fig. 8 for the LP case, which coincide with the dips mentioned in Fig. 5. According to the inset of Fig. 4, at $\omega = 0.4$ a.u. in LP case, the weights of some partial waves related to the nondipole transitions are apparently small, e.g., the $l = 2, m = \pm 1$ and $l = 3, m = \pm 1$ partial waves, which means some nondipole transitions are suppressed. On the contrary, in the CP case this obvious difference in weights of these partial waves does not appear in Fig. 4 and no minimum points exist in Fig. 8 either. Nevertheless, it remains an interesting question why the suppression of the nondipole transitions happens at these specific frequencies in the LP case, which deserves a further study.

V. THE COULOMB SCREENING EFFECT

In this section we turn to discuss the Coulomb screening effect on the photon-momentum transfer. The effect of the Coulomb tail and the influence of potentials on the initial states will be investigated. For these purposes, we will only focus on the single-photon ionization process in the linear polarization case.

We use similar laser parameters as before. Three different short-range potentials are considered, e.g., the Yukawa potential given by $V(r) = -Ze^{-\alpha r}/r$ ($Z = 1.905$, $\alpha = 1$ and $Z = 1.5$, $\alpha = 0.5365$), and the finite potential [54] given by $V(r) = -e^{-(r/10)^2}/r$. These potentials will result in the same ground state energy as the real H atom. From Fig. 9(c) first we can conclude the insignificancy of the Coulomb tail in this long-pulse single-photon ionization case through comparing the scaling law in the Coulomb potential and the finite potential because these two potentials coincide in the short range but deviate in the long range, as is shown in Figs. 9(a) and 9(b). Then the change of the scaling law between the finite potential and the Yukawa potential with different value of "Z" can

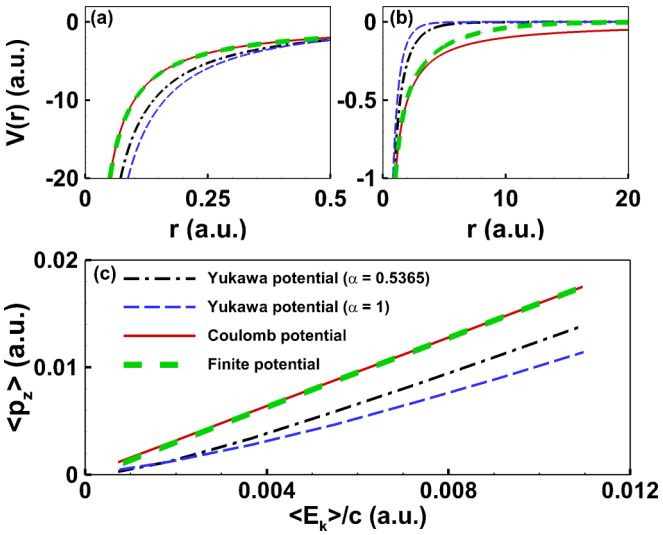

FIG. 9. Top panels show different types of potential $V(r)$ in the regime of (a) $0 < r < 0.5$ a.u. and (b) $0 < r < 20$ a.u. The lower panel shows the expectation of photoelectron momentum $\langle p_z \rangle$ along the laser propagation direction as a function of $\langle E_k \rangle / c$ in the one-photon ionization regime with different potential types. Red solid line: results with the Coulomb potential given by $V(r) = -1/r$; thick green dashed line: results with the finite potential; thin blue dashed line: results with the Yukawa potential ($Z = 1.905$, $\alpha = 1$); black dash-dotted line: results with the Yukawa potential ($Z = 1.5$, $\alpha = 0.5365$).

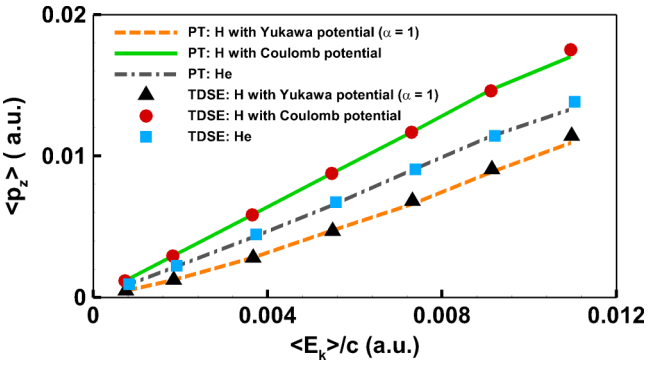

FIG. 10. The expectation of photoelectron momentum along the propagation direction $\langle p_z \rangle$ as a function of $\langle E_k \rangle / c$ in the one-photon ionization regime for three cases: hydrogen atom in the Coulomb potential (green solid line for PT and red solid circles for TDSE); hydrogen atom in the Yukawa potential ($Z = 1.905$, $\alpha = 1$) (yellow dashed line for PT and black solid triangles for TDSE); helium atom with a model potential (gray dash-dotted line for PT and blue solid squares for TDSE).

confirm the significant effects of the short-range part of the potential because these potentials coincide in the long range but deviate in the short range. For the Yukawa potential, the initial state is influenced by the factor Z, which will surely change the photon-momentum transfer rule.

Here we introduce a numerical calculation by the perturbation theory to support our speculation. The initial states can be extracted from the imaginary time propagation as mentioned in Sec. II. Thus the influence of different kinds of short-range potentials on the initial state can be included. Results from this numerical calculation for the H atom and the He atom are shown in Fig. 10, compared against the TDSE calculations. For the helium case, we use a model potential given by $V(r) = -\frac{1}{r}[1 + (1 + 27/16r)e^{-27/8r}]$ [55].

Both calculations indicate that the potential can affect the momentum transfer rules, namely the relationship between $\langle p_z \rangle$ and $\langle E_k \rangle / c$. Almost identical slopes are obtained from these two methods, which are no longer equal to 1.6 for the H atom in the Yukawa potential and the He atom in the model potential. Please note that the exact scattering wave has been used in our numerical calculations from the perturbation theory. We must point out here that although the plane wave approximation used in Ref. [37] seemed applicable in the calculation of the photon-momentum transfer of H atom during the single-photon ionization process, it may not be able to provide an accurate electron momentum distribution. We also find that the ionization probability under the plane wave approximation deviates from the TDSE results, although one can arrive at the same photon-momentum transfer law.

VI. CONCLUSIONS

For the photon-momentum transfer in the one- and two-photon case, we have solved the 3D time-dependent Schrödinger equation beyond the dipole approximation for a hydrogenlike system and introduced a numerical calculation from the perturbation theory with the exact scattering states. Our findings confirm the photon-momentum transfer rules and its polarization-independent characteristics in the single-photon ionization case. While in the two-photon ionization process, we discovered some distinct dips appearing at specific laser frequencies in the transfer of the photon linear momentum to the electron. These dips are dependent on the laser ellipticity, which disappear in the circular polarization cases. We attributed this to the different weights of nondipole transitions at various laser frequencies. Finally, we discussed the screening effect of the Coulomb potential on the photon-momentum transfer and pointed out that the Coulomb tail is negligible in the long-pulse single-photon ionization case while the short range of the potential may influence the initial state, which will change the photon-momentum transfer rule.

ACKNOWLEDGMENTS

This work is supported by National Natural Science Foundation of China (NSFC) under Grant No. 11574010 and by the National Program on Key Basic Research Project (973 Program) under Grant No. 2013CB922402.

[1] S. Palaniyappan, I. Ghebregziabher, A. DiChiara, J. MacDonald, and B. C. Walker, Phys. Rev. A **74**, 033403 (2006).
[2] H. R. Reiss, Phys. Rev. Lett. **101**, 043002 (2008).
[3] H. R. Reiss, J. Phys. B **47**, 204006 (2014).

[4] N. J. Kylstra, R. A. Worthington, A. Patel, P. L. Knight, J. R. Vázquez de Aldana, and L. Roso, Phys. Rev. Lett. **85**, 1835 (2000).
[5] M. Gavrila, J. Phys. B **35**, R147 (2002).
[6] A. M. Popov, O. V. Tikhonova, and E. A. Volkova, J. Phys. B **36**, R125 (2003).
[7] M. Førre, S. Selstø, J. P. Hansen, and L. B. Madsen, Phys. Rev. Lett. **95**, 043601 (2005).
[8] M. Y. Emelin and M. Y. Ryabikin, Phys. Rev. A **89**, 013418 (2014).
[9] A. S. Simonsen and M. Førre, Phys. Rev. A **92**, 013405 (2015).
[10] A. Staudt and C. H. Keitel, J. Phys. B **36**, L203 (2003).
[11] A. Staudt and C. H. Keitel, Phys. Rev. A **73**, 043412 (2006).
[12] B. Krässig, M. Jung, D. S. Gemmell, E. P. Kanter, T. LeBrun, S. H. Southworth, and L. Young, Phys. Rev. Lett. **75**, 4736 (1995).
[13] N. L. S. Martin, D. B. Thompson, R. P. Bauman, C. D. Caldwell, M. O. Krause, S. P. Frigo, and M. Wilson, Phys. Rev. Lett. **81**, 1199 (1998).
[14] V. K. Dolmatov and S. T. Manson, Phys. Rev. Lett. **83**, 939 (1999).
[15] A. Derevianko, O. Hemmers, S. Oblad, P. Glans, H. Wang, S. B. Whitfield, R. Wehlitz, I. A. Sellin, W. R. Johnson, and D. W. Lindle, Phys. Rev. Lett. **84**, 2116 (2000).
[16] O. Hemmers, H. Wang, P. Focke, I. A. Sellin, D. W. Lindle, J. C. Arce, J. A. Sheehy, and P. W. Langhoff, Phys. Rev. Lett. **87**, 273003 (2001).
[17] B. Krässig, E. P. Kanter, S. H. Southworth, R. Guillemin, O. Hemmers, D. W. Lindle, R. Wehlitz, and N. L. S. Martin, Phys. Rev. Lett. **88**, 203002 (2002).
[18] O. Hemmers, R. Guillemin, E. P. Kanter, B. Krässig, D. W. Lindle, S. H. Southworth, R. Wehlitz, J. Baker, A. Hudson, M. Lotrakul, D. Rolles, W. C. Stolte, I. C. Tran, A. Wolska, S. W. Yu, M. Y. Amusia, K. T. Cheng, L. V. Chernysheva, W. R. Johnson, and S. T. Manson, Phys. Rev. Lett. **91**, 053002 (2003).
[19] O. Hemmers, R. Guillemin, D. Rolles, A. Wolska, D. W. Lindle, E. P. Kanter, B. Krässig, S. H. Southworth, R. Wehlitz, B. Zimmermann, V. McKoy, and P. W. Langhoff, Phys. Rev. Lett. **97**, 103006 (2006).
[20] M. Førre, Phys. Rev. A **74**, 065401 (2006).
[21] M. Førre, J. P. Hansen, L. Kocbach, S. Selstø, and L. B. Madsen, Phys. Rev. Lett. **97**, 043601 (2006).
[22] Z. Zhou and S.-I. Chu, Phys. Rev. A **87**, 023407 (2013).
[23] M. Førre, S. Selstø, J. P. Hansen, T. K. Kjeldsen, and L. B. Madsen, Phys. Rev. A **76**, 033415 (2007).
[24] A. Y. Istomin, N. L. Manakov, A. V. Meremianin, and A. F. Starace, Phys. Rev. Lett. **92**, 063002 (2004).
[25] A. Y. Istomin, N. L. Manakov, A. V. Meremianin, and A. F. Starace, Phys. Rev. A **71**, 052702 (2005).
[26] A. Y. Istomin, A. F. Starace, N. L. Manakov, A. V. Meremianin, A. S. Kheifets, and I. Bray, J. Phys. B **39**, L35 (2006).
[27] N. A. Cherepkov and S. K. Semenov, J. Phys. B **34**, L211 (2001).
[28] N. A. Cherepkov and S. K. Semenov, J. Phys. B **34**, L495 (2001).
[29] T. Khalil, B. Schmidtke, M. Drescher, N. Müller, and U. Heinzmann, Phys. Rev. Lett. **89**, 053001 (2002).
[30] C. T. L. Smeenk, L. Arissian, B. Zhou, A. Mysyrowicz, D. M. Villeneuve, A. Staudte, and P. B. Corkum, Phys. Rev. Lett. **106**, 193002 (2011).
[31] A. S. Titi and G. W. F. Drake, Phys. Rev. A **85**, 041404 (2012).
[32] M. Klaiber, E. Yakaboylu, H. Bauke, K. Z. Hatsagortsyan, and C. H. Keitel, Phys. Rev. Lett. **110**, 153004 (2013).
[33] H. R. Reiss, Phys. Rev. A **87**, 033421 (2013).
[34] J. Liu, Q. Z. Xia, J. F. Tao, and L. B. Fu, Phys. Rev. A **87**, 041403 (2013).
[35] E. Yakaboylu, M. Klaiber, H. Bauke, K. Z. Hatsagortsyan, and C. H. Keitel, Phys. Rev. A **88**, 063421 (2013).
[36] A. Ludwig, J. Maurer, B. W. Mayer, C. R. Phillips, L. Gallmann, and U. Keller, Phys. Rev. Lett. **113**, 243001 (2014).
[37] S. Chelkowski, A. D. Bandrauk, and P. B. Corkum, Phys. Rev. Lett. **113**, 263005 (2014).
[38] S. Chelkowski, A. D. Bandrauk, and P. B. Corkum, Phys. Rev. A **92**, 051401 (2015).
[39] I. A. Ivanov, Phys. Rev. A **91**, 043410 (2015).
[40] D. Cricchio, E. Fiordilino, and K. Z. Hatsagortsyan, Phys. Rev. A **92**, 023408 (2015).
[41] D. Lao, P.-L. He, and F. He, Phys. Rev. A **93**, 063403 (2016).
[42] J. F. Tao, Q. Z. Xia, J. Cai, L. B. Fu, and J. Liu, Phys. Rev. A **95**, 011402 (2017).
[43] P.-L. He, D. Lao, and F. He, Phys. Rev. Lett. **118**, 163203 (2017).
[44] S. Chelkowski, A. D. Bandrauk, and P. B. Corkum, Phys. Rev. A **95**, 053402 (2017).
[45] M. W. Walser, C. H. Keitel, A. Scrinzi, and T. Brabec, Phys. Rev. Lett. **85**, 5082 (2000).
[46] N. J. Kylstra, R. M. Potvliege, and C. J. Joachain, J. Phys. B **34**, L55 (2001).
[47] M. Førre and A. S. Simonsen, Phys. Rev. A **90**, 053411 (2014).
[48] L.-Y. Peng and A. F. Starace, J. Chem. Phys. **125**, 154311 (2006).
[49] L.-Y. Peng, W.-C. Jiang, J.-W. Geng, W.-H. Xiong, and Q. Gong, Phys. Rep. **575**, 1 (2015).
[50] D. Bauer and P. Koval, Comput. Phys. Commun. **174**, 396 (2006).
[51] A. F. Starace, *Theory of Atomic Photonionization*, Handbuch der Physik/Encyclopedia of Physics, Vol. 31 (Springer, Berlin, 1982).
[52] H. Gouraud, IEEE Trans. Comput. **C-20**, 623 (1971).
[53] M. J. Seaton, J. Phys. B **29**, 2373 (1996).
[54] O. I. Tolstikhin and T. Morishita, Phys. Rev. A **86**, 043417 (2012).
[55] L.-Y. Peng, E. A. Pronin, and A. F. Starace, New J. Phys. **10**, 025030 (2008).